Coupled Systems Mechanics, *Vol. 10, No. 5 (2021) 371-392*
https://doi.org/10.12989/csm.2021.10.5.371

Coupled arch dam-reservoir-massed foundation problem under different earthquake input mechanisms

M. Varmazyari[a], S.R. Sabbagh-Yazdi[b] and H. Mirzabozorg*

Structural Engineering Department, Faculty of Civil Engineering, K. N. Toosi University of Technology, Tehran, Iran

(Received April 29, 2019, Revised June 12, 2021, Accepted July 9, 2021)

Abstract. The aim of the present study is to investigate a coupled arch dam-reservoir-massed foundation problem under two earthquake input mechanisms. The problem nonlinearity originates from opening/slipping of the vertical contraction joints of the dam body. The reservoir-structure interaction is taken into account assuming compressible reservoir. Also, the meshing approach (structured mesh vs. unstructured one) in the foundation medium is investigated. The Karoun-I double curvature arch dam is selected as a case study. Three components of the 1994 Northridge earthquake are selected as the free-field ground motion. A deconvolution analysis in 3D space is conducted to adjust the amplitude and frequency contents of the earthquake ground motion applied to the bottom of the massed foundation to determine the desired acceleration response at various points on the dam-foundation interface taking into account the coupling between the foundation and the structure. It is found that in the deconvolved earthquake input models, the maximum tensile and the compressive stresses increase by 19% and 12%, respectively in comparison with those of the free-field input models. In addition, modeling foundation using the unstructured mesh decreases the maximum compressive stresses within the dam body by about 20% in comparison with that obtained using the structured mesh model. In the same way, the maximum crest displacements in the horizontal direction decreases by about 30%.

Keywords: 3D earthquake excitation; coupled dam-reservoir-massed foundation; deconvolution; unstructured meshing

1. Introduction

The accurate and reasonable coupling of an arch dam and its surrounding foundation and proper modeling of input ground motions have been the subjects of many researches in recent years (Chuhan *et al*. 2009, Pan *et al*. 2009). Generally, four different models of earthquake input mechanism are recognized to analyze the coupled problem of dam-reservoir-foundation, which are: rigid foundation model; massless foundation model; free-field acceleration input; and deconvolved earthquake input. The rigid base model and massless foundation model overestimate seismic response of the dam-foundation problem (Léger and Boughoufalah 1989, USBR 2002). In the case of free-field acceleration input model, acceleration is directly applied to the dam-foundation

*Corresponding author, Associate Professor, E-mail: mirzabozorg@kntu.ac.ir
[a]Ph.D. Candidate, E-mail: mvarmazyar@dena.kntu.ac.ir
[b]Professor, E-mail: syazdi@kntu.ac.ir

http://www.techno-press.org/?journal=csm&subpage=8 ISSN: 2234-2184 (Print), 2234-2192 (Online)

interface (Hariri Ardebili and Saouma 2013). However, this model ignores spatial variation of the ground motions (Huang and Zerva 2014). Finally, in the case of the deconvolved earthquake input model, the earthquake applied to the base of the foundation is adjusted to obtain the desired acceleration at the dam-foundation interface. The computer program, SHAKE (Schnabel *et al*. 1972) has widely been used for deconvolution in the previous studies. However, this program is very cumbersome because the response by the deconvolution process is extremely affected by values of the shear modulus and the equivalent viscous damping ratio in flexible foundations (Léger and Boughoufalah 1989). Sooch and Bagchi (2012) presented a modified deconvolution procedure for seismic assessment of the coupled problem of concrete gravity dam-foundation.

On the other hand, mesh type in finite element modelling in order to achieve more accuracy in seismic response in the coupled problem of dam-foundation is a state-of-the-art research problem in dam engineering field. This is due to several factors such as the element's shape and its distortion that may affect the results in a finite element solution. In modelling a foundation as a structured mesh, high aspect ratio elements commonly appear in some coarse meshing parts on far end boundaries of the foundation in contrary to the fine mesh when approaching to the dam body. Theoretical reason for having less accuracy for high aspect ratio elements can be understood from the computational method in finite element modelling (Javidinejad 2012). In 3D meshing, tetrahedral and hexahedral are two most commonly used elements. The results obtained by these two elements can differ remarkably due to bad-shaped and high aspect ratio elements. A few studies have already been carried out comparing hexahedral versus tetrahedral meshes. For instance, Owen (1998) provided an overview of many techniques comparing hexahedral and tetrahedral meshes. In addition, Benzley *et al*. (1995) while comparing the performance of hexahedral vs. tetrahedral elements showed that the stiffness matrix eigenvalues for linear tetrahedrons were larger than those for linear hexahedrons and hexahedral elements. They also demonstrated that the linear hexahedral elements deform in a lower strain energy state making them more accurate than linear tetrahedrons. The most important advantage of hexahedral elements is where the non-trivial boundaries are required and obtained by breaking the region up into topological blocks (Chandrupatla *et al*. 2002). Carl *et al*. (2006) studied the performance of elastic solid FE modelling using both hexagonal and tetrahedral meshes. Based on the study conducted by Ramos and Simões (2005), linear tetrahedral elements yield results which are close to the theoretical values. Diwan and Mahajan (2017) studied the results of stress analysis obtained using different mesh types. Also, Hadzalic *et al*. (2018) studied effects of two mesh type of triangular elements on the response of a soil-foundation system. Based on their results, after first cracking the responses for two different types of coarse and fine meshes start to differ. Ziaolhagh *et al*. (2016) investigated analysis of a gravity dam-reservoir problem utilizing different triangular elements. On the other hand, linear hexahedral elements are sensible with respect to the corner angle. Quadratic hexahedral elements are very robust, but computationally expensive (Wang *et al*. 2004). Cifuentes and Kalbag (1992) found that both quadratic tetrahedral elements and bilinear hexahedral elements yield equivalent results in terms of accuracy and CPU time. Weingarten (1994) showed that quadratic tetrahedrons and hexahedrons were equivalent in accuracy.

Tetrahedral elements for modelling the foundation subjected to seismic loading have been used by some researchers (Andonov *et al*. 2012, Lemos 2012, Buffi 2017, Vezi 2014). However, a very few studies have been published to investigate the effects of hexahedral versus tetrahedral meshes on results. Saouma *et al*. (2001) studied Statistical finite element analysis of an existing arch dam surrounded by the rock foundation. They stated "there is no reason to suggest that brick elements yield more accurate results than tetrahedron". Gracia Llinares (2016) compared the results accuracy

obtained using tetrahedral elements with those using hexahedral elements conducting a thermo-mechanical analysis on a dam-foundation model. Jin *et al*. (2019) investigated the effects of foundation modelling on seismic response of arch dams. However, the earthquake response of a typical arch dam considering different mesh types of the massed foundation is absent from the literature.

The present paper aims to study on a comprehensive provided coupled reservoir-dam-massed foundation problem including structural nonlinearity to examine the effect of meshing of the surrounding foundation on the seismic response of the dam subjected to different earthquake input mechanisms. The reservoir-structure interaction is taken into account using and Eulerian finite element formulation incorporating appropriate boundary conditions applied on the compressible reservoir domain. For more accurate and realistic modelling the structure-foundation interaction, the foundation medium is assumed to be massed and therefore, the mechanism for applying the input ground motion and absorption of the outgoing waves on the far-end boundaries of the surrounding rock are important. The nonlinearity originates from opening/slipping in vertical contraction joints within the dam body. At last, the effect of structured meshing of the massed foundation vs. an unstructured mesh of the surrounding rock on the seismic response of the dam body is investigated.

2. Formulation and solution technique

2.1 Fluid-structure-interaction

Considering the coupled dam-reservoir-foundation system, the governing equation in the reservoir medium is the Helmoltz equation as

$$\nabla^2 p = \frac{1}{C^2} \frac{\partial^2 p}{\partial t^2} \tag{1}$$

where p, C, and t are the hydrodynamic pressure, pressure wave velocity in liquid domain, and time, respectively. The partial absorptive boundary is applied on the reservoir around, and the Sommerfeld boundary is applied to the far end truncated of the reservoir. Other boundary conditions to solve Eq. (13) can be found in (Hariri-Ardebili *et al*. 2013). The governing equations of the structure and reservoir take the form as

$$\begin{bmatrix} [M] & 0 \\ \rho[Q]^T & [G] \end{bmatrix} \begin{Bmatrix} \ddot{U} \\ \ddot{P} \end{Bmatrix} + \begin{bmatrix} [C] & 0 \\ 0 & [C'] \end{bmatrix} \begin{Bmatrix} \dot{U} \\ \dot{P} \end{Bmatrix} + \begin{bmatrix} [K] & -[Q] \\ 0 & [K'] \end{bmatrix} \begin{Bmatrix} U \\ P \end{Bmatrix} = \begin{Bmatrix} \{f_1\} - [M]\{\ddot{U}_g\} \\ \{F\} - \rho[Q]^T \{\ddot{U}_g\} \end{Bmatrix} \tag{2}$$

where $[M]$, $[C]$, and $[K]$ are the mass, damping, and stiffness matrices of the structure including the dam body and its surrounding foundation rock. Also, $[G]$, $[C']$, and $[K']$ are the matrices representing the mass, damping, and stiffness equivalent matrices of the reservoir, respectively. In addition, $[Q]$ is the coupling matrix; $\{f_1\}$ is the force vector including both body and hydrostatic force; $\{P\}$ and $\{U\}$ are the vectors of hydrodynamic pressures and displacements, respectively, and $\{\ddot{U}_g\}$ is the ground acceleration vector. $\{F\}$ is the force vector due to integration on all the reservoir boundaries. $\{\dot{P}\}$ and $\{\ddot{P}\}$ are the first and second time derivatives of the nodal hydrodynamic pressure vector, respectively, and ρ is the water density. It is worth noting that the stiffness and mass proportional damping equivalent to 10% of the critical damping based on the 2Hz and 6Hz frequencies of the dam-foundation system is applied to the structure (Hall 2006).

2.2 Foundation interaction and wave propagation

The equations governing *P* and *S* waves propagating within the massed foundation rock are given as

$$\frac{\partial^2 u}{\partial t^2} = V_p^2 \nabla^2 u \tag{3}$$

$$\frac{\partial^2 v}{\partial t^2} = V_s^2 \nabla^2 v \tag{4}$$

$$\frac{\partial^2 w}{\partial t^2} = V_s^2 \nabla^2 w \tag{5}$$

in which, u, v, and w are the displacements in the direction of wave propagation and two other orthogonal directions, respectively, and V_p, and V_s are primary and secondary wave propagation velocities within the rock medium derived as

$$V_p = \sqrt{\frac{E_r (1-\upsilon_r)}{\rho_r (1+\upsilon_r)(1-2\upsilon_r)}} \tag{6}$$

$$V_s = \sqrt{\frac{G_r}{\rho_r}} = \sqrt{\frac{E_r}{2(1+\upsilon_r)\rho_r}} \tag{7}$$

where E, G, υ, and ρ are the modulus of elasticity, shear modulus, Poisson's ratio, and density, respectively, and subscript r indicates that the parameters are pertinent to the foundation rock (Mirzabozorg *et al*. 2007).

One of the main aspects in seismic loading and wave propagation within the semi-infinite medium such as the rock underlying structures is prevention of wave reflection from the artificial boundary on the far end nodes into the finite element model. In this study, Lysmer's viscous boundary, which is a non-consistent boundary is applied to the far-end nodes of the foundation in 3D space as following

$$\sigma = \rho_r V_P \dot{u} \tag{8}$$

$$\tau_1 = \rho_r V_S \dot{v} \tag{9}$$

$$\tau_2 = \rho_r V_S \dot{w} \tag{10}$$

where σ, τ_1, and τ_2 are the normal and two in-plane shear stresses in the global directions, respectively. Radiation damping derived from Eqs. (8)-(10) which are applied to the far-end boundary of the foundation is made up of dashpots that are added to the global damping matrix of the structure, [C]. In the present research, these lumped dashpots are determined as (Mirzabozorg *et al*. 2007)

$$C_{11}^i = V_P \rho_r \int_{A_e} N_i dA \tag{11}$$

$$C_{22}^i = V_S \rho_r \int_{A_e} N_i dA \tag{12}$$

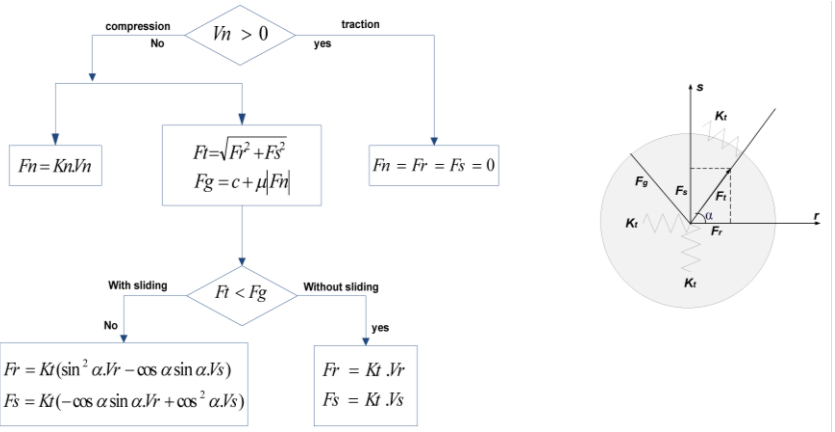

Fig. 1 Flowchart for calculating forces in joints (Hariri-Ardebili and Mirzabozorg 2012)

$$C_{33}^{i} = V_S \rho_r \int_{A_e} N_i dA \tag{13}$$

where, C_{11}^{i}, C_{22}^{i}, and C_{33}^{i} are components of the lumped damping applied to the i^{th} node of the element on the far end boundary of the surrounding rock in normal and two orthogonal tangential directions, respectively; N_i is the i^{th} node shape function; and all integrations are applied over the area of considered surface of the element, A_e (Mirzabozorg *et al*. 2007).

2.3 Joint nonlinearity

In the present study, a special contact element is used to model the contraction joints, which is able to model the contact between two adjacent nodes in 3D space. This contact element supports compression in the normal direction and shears in the two orthogonal tangential directions. Fig. 1 shows the flowchart used for calculating force in contact elements. In the figure, V is a vector representing the relative displacements of the coincident nodes located on the joint surface in the local directions indicating the contact state in various directions so that V_n which is normal relative displacement indicates the open/close state of the joint; Also, V_r and V_s indicate the state of the considered contact element in the tangential directions. Moreover, Fig. 2 depicts force deflection relations for both the normal and tangential status. In this flowchart, F_n, F_r, and F_s are the local components of the force vector; F_g is the sliding force in the joint; F_t is the shear force resultant in the joint; K_n and K_t are the normal and tangential stiffness of the joint and α is the angle between the two components of in-plane shears (Hariri-Ardebili and Mirzabozorg 2012).

It should be noted that F_g in Fig. 2(b) is equal to F_n multiplied by a friction coefficient. As shown, the contact element cannot endure any tensile force or stress but when it is in compression, it can suffer compression forces according to its normal stiffness and shear forces according to its tangential stiffness. When the shear force resultant in the joint exceeds the joint sliding resisting force, the two nodes of the element begin sliding with respect to each other. The joint sliding force is calculated using the coulomb friction law. In Fig. 1, c is the cohesion factor and μ is the friction coefficient. Usually, in concrete dams the cohesion factor is assumed to be zero because of its negligible effect on the results. Also the friction coefficient is assumed to be unity so that the friction angle is 45° (Hariri-Ardebili and Mirzabozorg 2012).

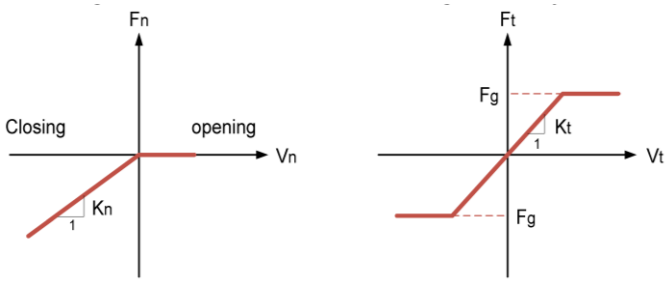

Fig. 2 Force-deflection relations for joint: (a) normal opening; (b) tangential movement (Hariri-Ardebili and Mirzabozorg 2012)

Fig. 3 Aerial view of Karoun-I double curvature arch dam

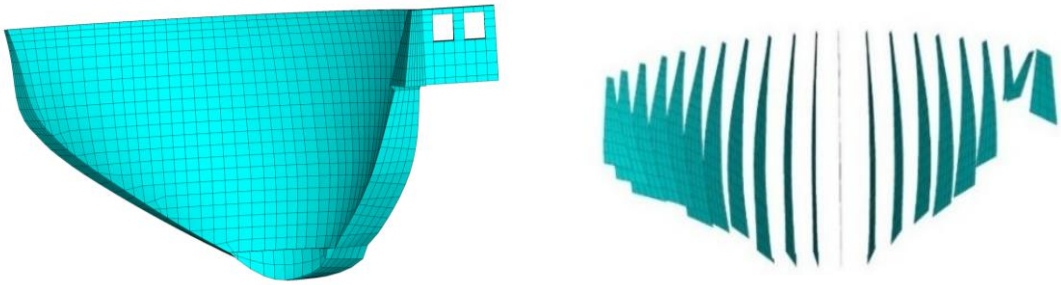

(a) (b)

Fig. 4 Finite element model: (a) Dam body (b) Contraction joints

3. Finite element model

Karoun-I dam is a 200 m high double curvature arch dam constructed on Karun River in Khuzestan province of Iran (Fig. 3). Thickness of the dam at the crest is 6 m and its maximum thickness at the base is 33.5 m, and its length along the crest is 380 m. The finite element model prepared in ANSYS software (2007) for the dam, contraction vertical joints, and water is presented in Fig. 4. Also, Fig. 5 illustrates the finite element model of the dam-reservoir-foundation system with the structured and unstructured mesh generation of the foundation.

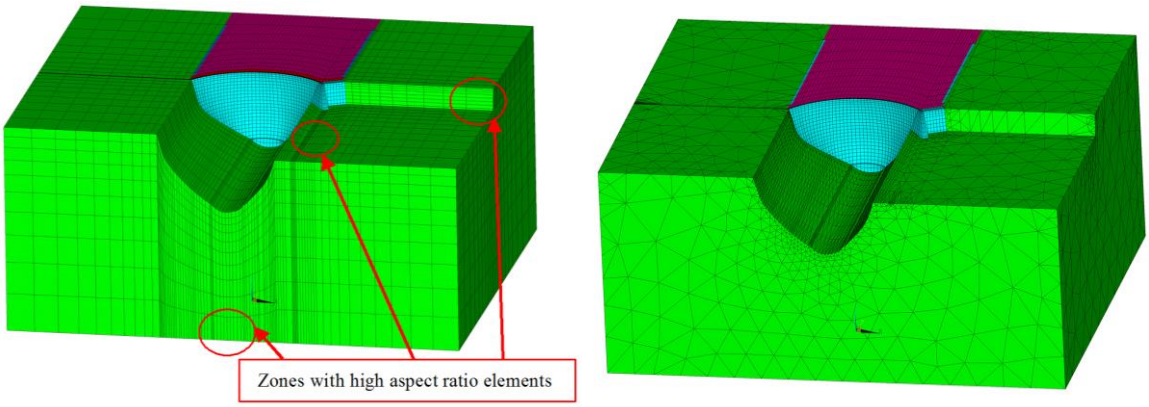

(a) Fully structured mesh model (b) Unstructured-structured mesh model

Fig. 5 Finite element model of the dam-reservoir-foundation system

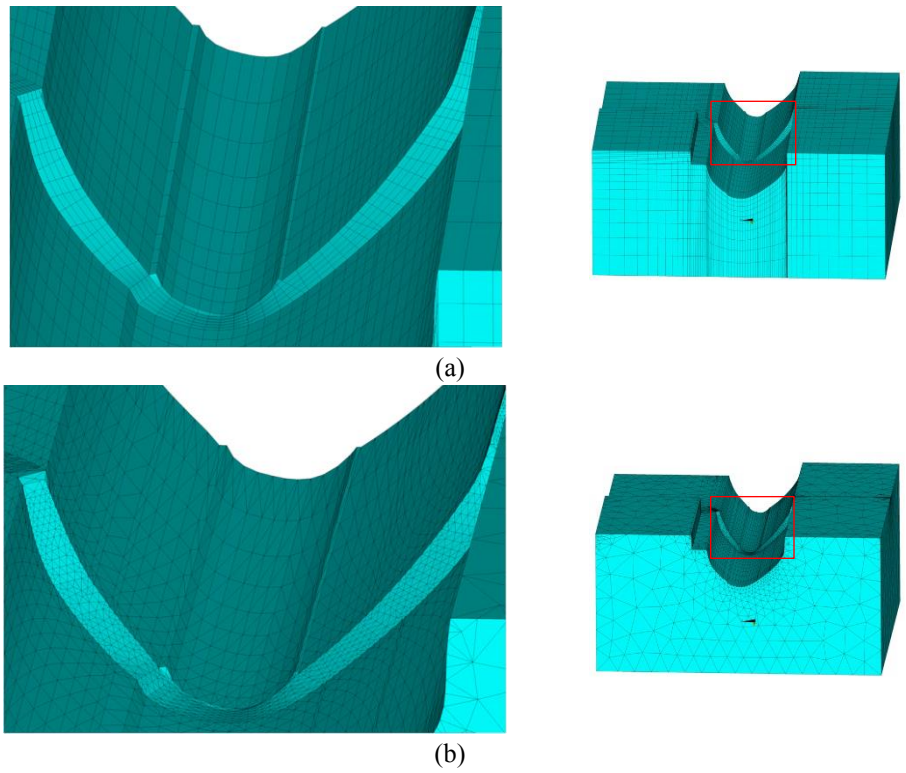

(a)

(b)

Fig. 6 Dam-foundation interface zone; (a) The structured mesh foundation; (b) Unstructured mesh foundation

Generally, in arch dams the dimensions of the foundation are at least twice as much as the dam height (consistent with topography of the site) to diminish the effects of the far end boundary conditions on the response of the dam body. The provided model consists of 3987 8-node solid elements to make the dam body, and its spillway and the thrust block and 23270 8-node solid elements to form the surrounding foundation rock. In order to reduce the unfavourable effects of

high aspect ratio elements (which inherently appear in the foundation part of the structured mesh, Fig. 5(a)) on the finite element results, the unstructured meshing strategy is considered for the foundation as well. The unstructured mesh foundation is formed using 37645 tetrahedral solid elements. It is worth noting that 2% and 14% of the elements violate shape warning limits (including quantities of aspect ratio and maximum corner angle) in the structured and unstructured mesh models, respectively.

The utilized 8-node solid elements have three translational degrees of freedom at each node. In addition, water is modeled using 7770 8-node fluid elements having three translational DOFs and one pressure DOF in each node. It should be noted that translational DOFs are active only at nodes that are on the interfaces of solid elements. In addition, 2082 contact elements are used for modelling the contraction vertical joints. In order to link the unstructured mesh of the foundation to the structured mesh of the dam body, the foundation is modeled as mesh free using tetrahedral elements, so no node unconnected to the pertinent elements at the dam foundation interface remains. Fig. 6 exhibits the dam-foundation interface zone for the structured and unstructured mesh foundation. The material properties for mass concrete and its surrounding foundation are described in Table 1 (Mirzabozorg 2014). It is noteworthy that all the dam body and joint grouting were modeled considering the construction staging effects, as reported in as-built drawings. The strategy for static analysis can be addressed in (Sevim *et al*. 2014).

Table 1 Material properties for mass concrete, foundation rock, and reservoir (Mirzabozorg 2014)

Label	Static	Dynamic
$E_{concrete}$ (GPa)	30	30*1.15
$\rho_{concrete}$ (kg/m^3)	2400	2400
$\upsilon_{concrete}$	0.20	0.14
$f_t^{concrete}$(MPa)	3.9	3.9*1.5
$f_c^{concrete}$ (MPa)	40	41.8
$^*E_{rock}$ (GPa)	13~15	13~15
ρ_{rock} (kg/m^3)	2500	2500
υ_{rock}	0.25	0.25
C_{water} (m/s)	1440	1440
ρ_{water} (kg/m^3)	1000	1000

*Modulus of deformation

Normal and tangential stiffness for contact elements are taken as 200 GPa/m, and 20 GPa/m, respectively. These stiffness coefficients lead to reasonable opening/closing and sliding in contraction joints (Mirzabozorg 2014). The wave reflection coefficient for the reservoir rounding boundaries is assumed to be 0.8, conservatively (FERC 1999). It is worth noting that the calibration and validity of the FE model under thermal, self-weight, and hydrostatic loads was previously considered through comparing the results obtained from the model with those calculated during the monitoring procedure of the dam body as reported by Ramezani *et al*. (2017).

In the current study, the first 20s of three earthquake components recorded at Pacoima dam station during the Northridge earthquake on 17 Jan 1994 are selected for dynamic analyses (PEER 2016). The horizontal and vertical PGA's are 0.3 g, 0.43 g, and 0.17 g, respectively. All three

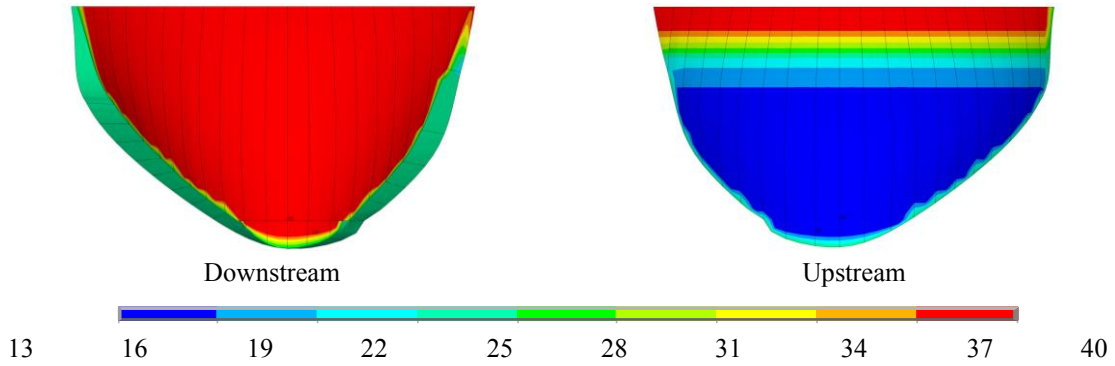

Fig. 7 Temperature distribution in summer on the downstream and upstream faces of the dam body (in ºC)

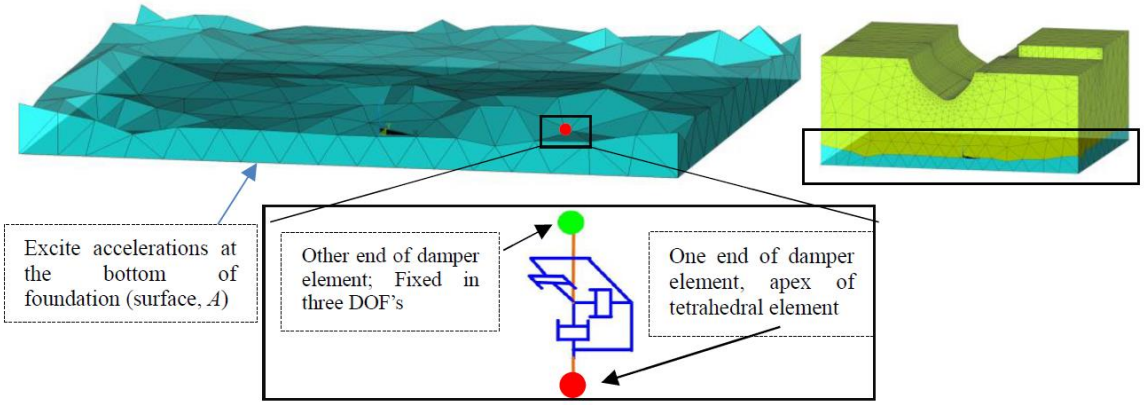

Fig. 8 Schematic of viscous boundary condition at the base of Finite Element model of the foundation

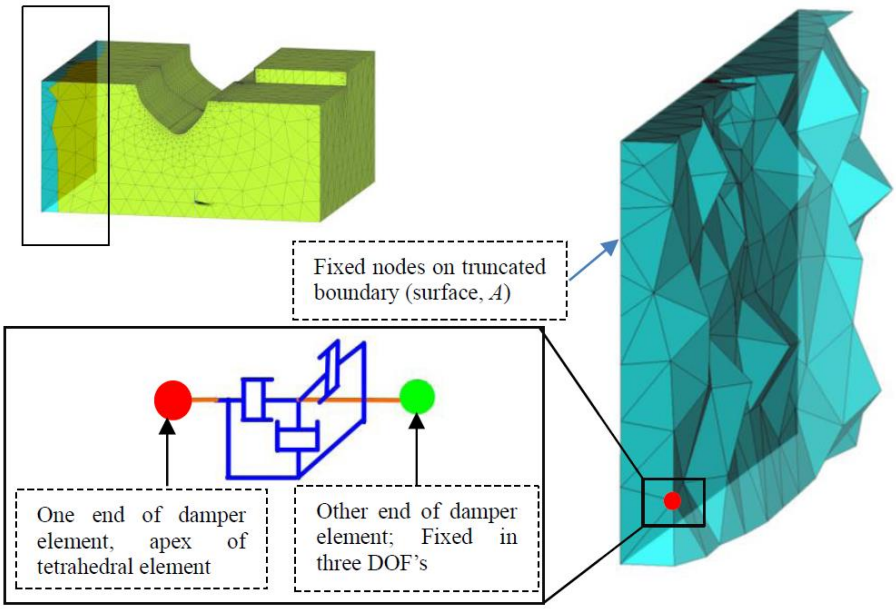

Fig. 9 Schematic of viscous boundary condition at the vertical truncated boundaries of the foundation

components are applied to the provided finite element model, simultaneously at the foundation base. It is worth noting that the summer loading conditions corresponding to the reservoir normal water level and the temperature distribution corresponding to that level, are applied to all the conducted analyses before exciting the models in seismic condition. The nodal temperature obtained from conducted transient thermal analyses discussed in (Ramezani *et al*. 2017) is applied to the dam body. Fig. 7 shows temperature distribution in summer conditions on the downstream and upstream faces of the dam body.

At last, Figs. 8 and 9 show the schematic of viscous boundary condition applied on the foundation base and vertical boundaries.

4. Deconvolved earthquake input model

4.1 Existing and modified deconvolution procedures

The Deconvolution adjust the amplitude and frequency contents of a record applied to the base of the foundation to achieve the desired acceleration at the dam-foundation interface. Fig. 10 shows the schematic of the deconvolution procedure for finite element analysis of the foundation model.

A step-by-step procedure for existing deconvolution is illustrated in Fig. 11 (Sooch and Bagchi 2012). The existing procedure works well for the low frequency ground motion records. However, in order to obtain an appropriate result for high frequency ground motion records a modified procedure has been used (Sooch and Bagchi 2012). Fig. 12 exhibits a flow chart for the modified deconvolution procedure.

Similarly, in modified procedure, the reproduced acceleration history at the reference point is compared to the free-field acceleration in frequency domain. However, Instead of Fourier amplitudes, the response spectra at different frequencies are adjusted in order to calculate the correction factors. The correction factors are calculated for each frequency by the ratio of the target

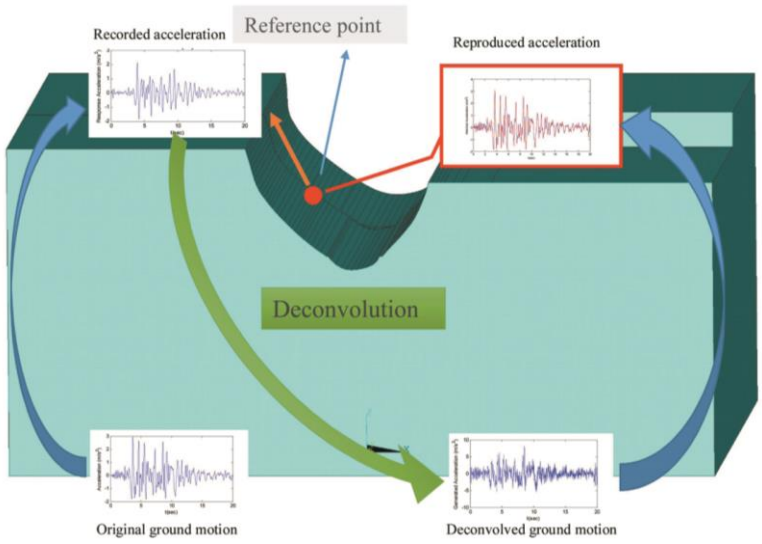

Fig. 10 Schematic of the deconvolution procedure

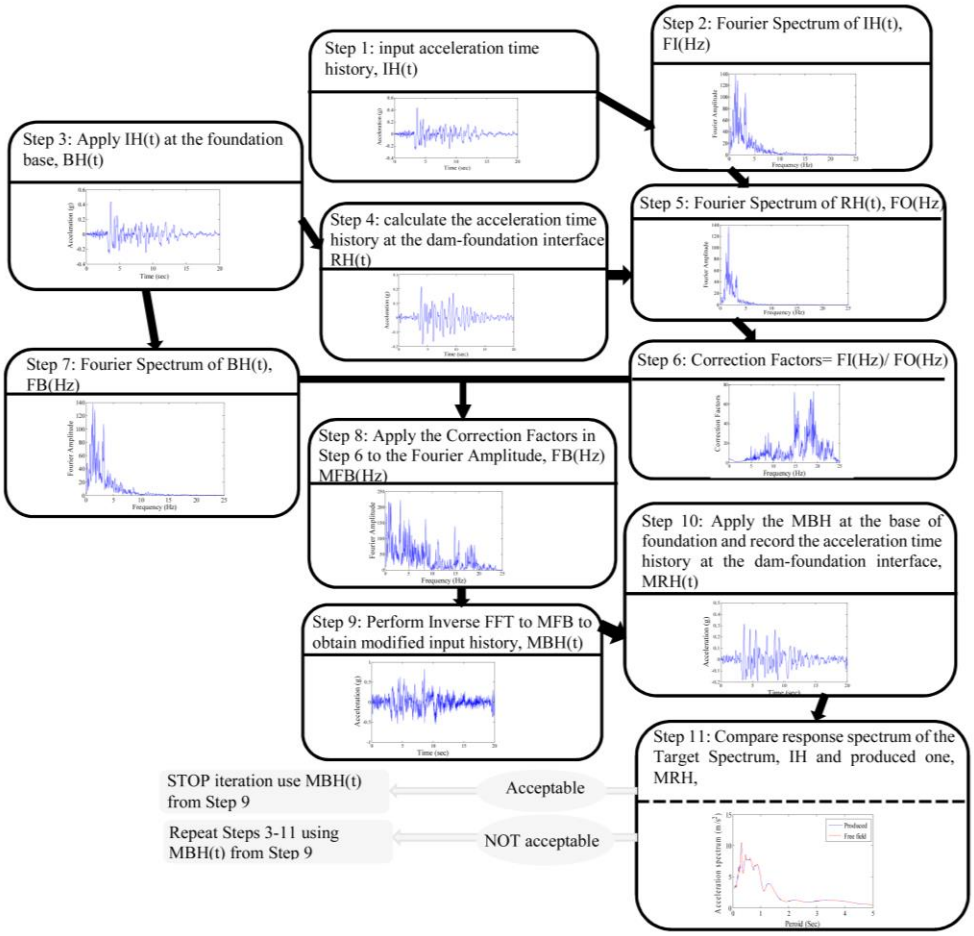

Fig. 11 Existing deconvolution procedure (Sooch and Bagchi 2012)

response spectrum amplitude and the response spectrum amplitude of the reproduced acceleration (Sooch and Bagchi 2012).

The complex Fourier coefficients of the acceleration signal applied to the base of the foundation model (real and imaginary part) are separately multiplied by the correction factor for each frequency to be complex conjugate. Similarly, after transforming back the modified acceleration signal to a time domain, the dam-reservoir-foundation system is excited with the modified acceleration time history at the base of the foundation. It is worth noting that in the present study, the results of the step-by-step deconvolution procedures are included in subplots of Figs. 11 and 12.

4.2 Accuracy of the deconvolution procedure

The reference point for the deconvolution analysis is selected to be located in the lower ¼ height of the dam on the dam-foundation interface (see Fig. 10). Fig. 13 compares the response accelerations on reference point and the corresponding free-field ground motions in three directions. Also, to investigate accuracy of the procedure, the comparison of the response spectra of

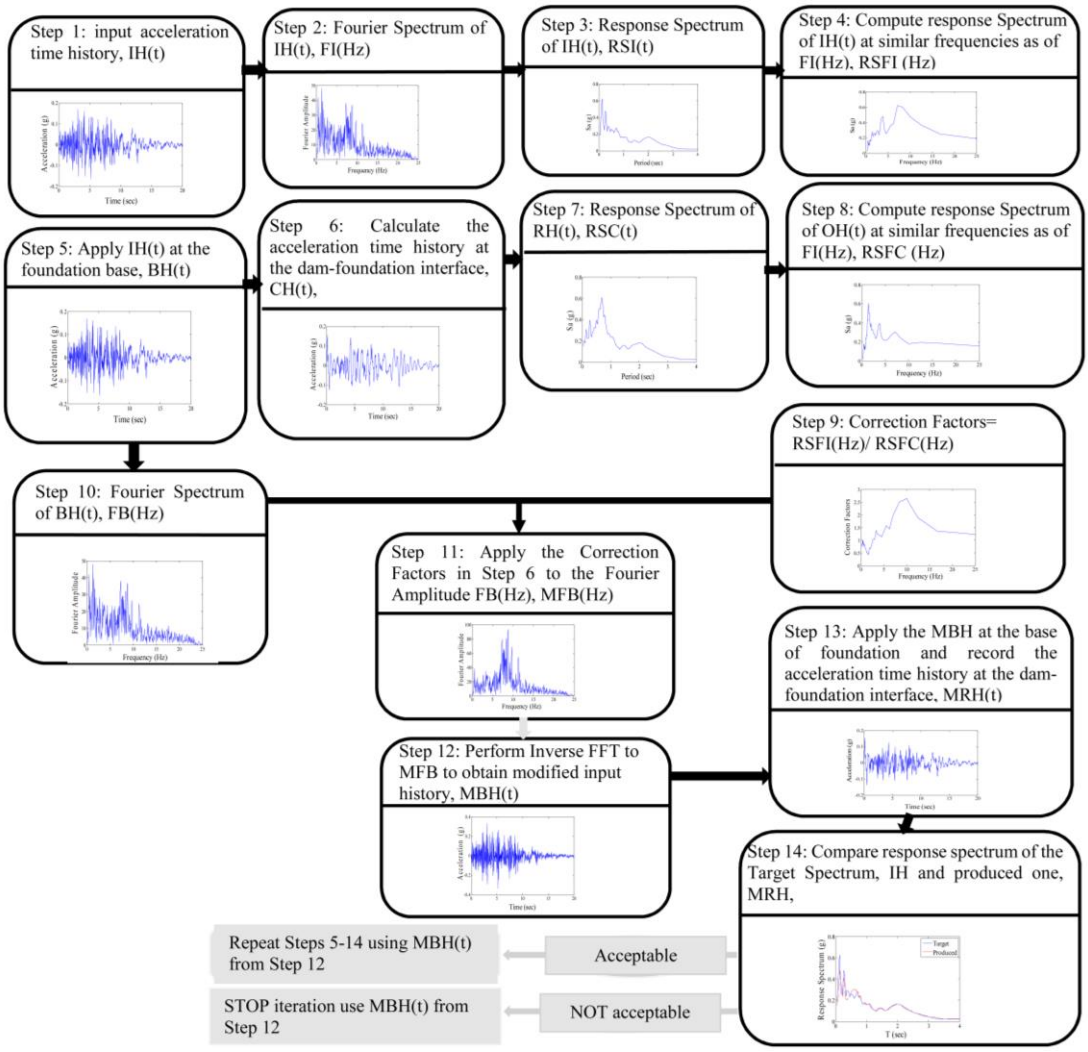

Fig. 12 Modified deconvolution procedure (Sooch and Bagchi 2012)

deconvolved earthquake ground acceleration on the reference point with the corresponding target ones for the unstructured foundation is shown in Fig. 14. As can be seen, the results match completely in the two horizontal directions. The modified deconvolution procedure, which has been used for vertical ground motions leads to more accurate result.

5. Conducted dynamic analyses

Four cases are considered in the analyses which are: deconvolved earthquake input models with the structured and unstructured foundations (models I and II, respectively); the free-field acceleration input models with the structured and unstructured foundation; (models III and IV, respectively).

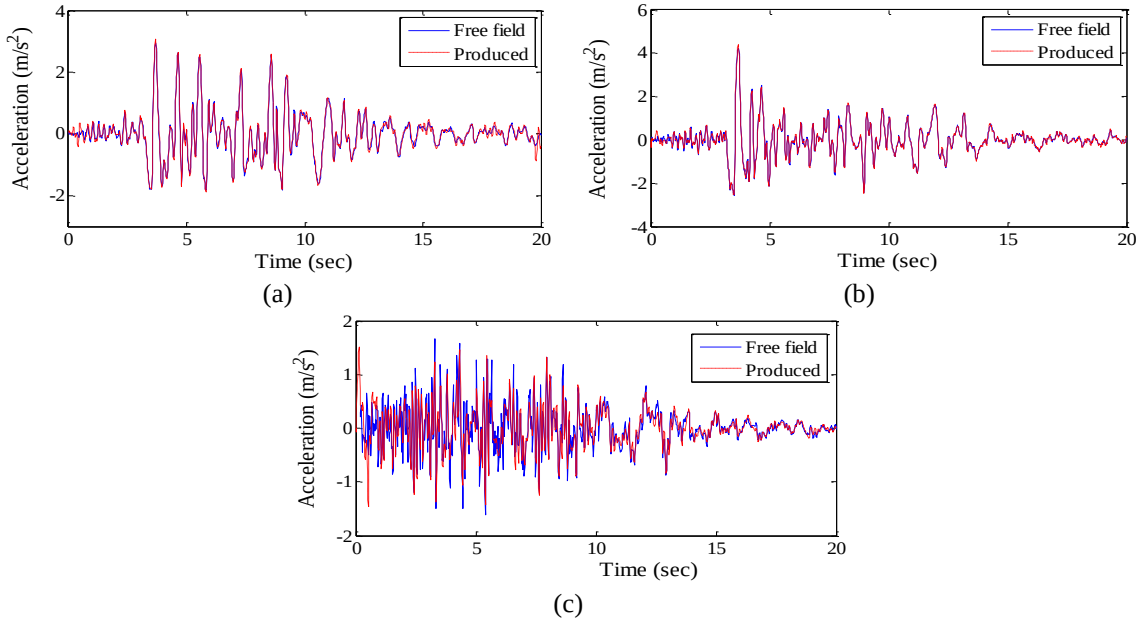

Fig. 13 Comparison between the response accelerations on reference point and the corresponding free-field ground motions

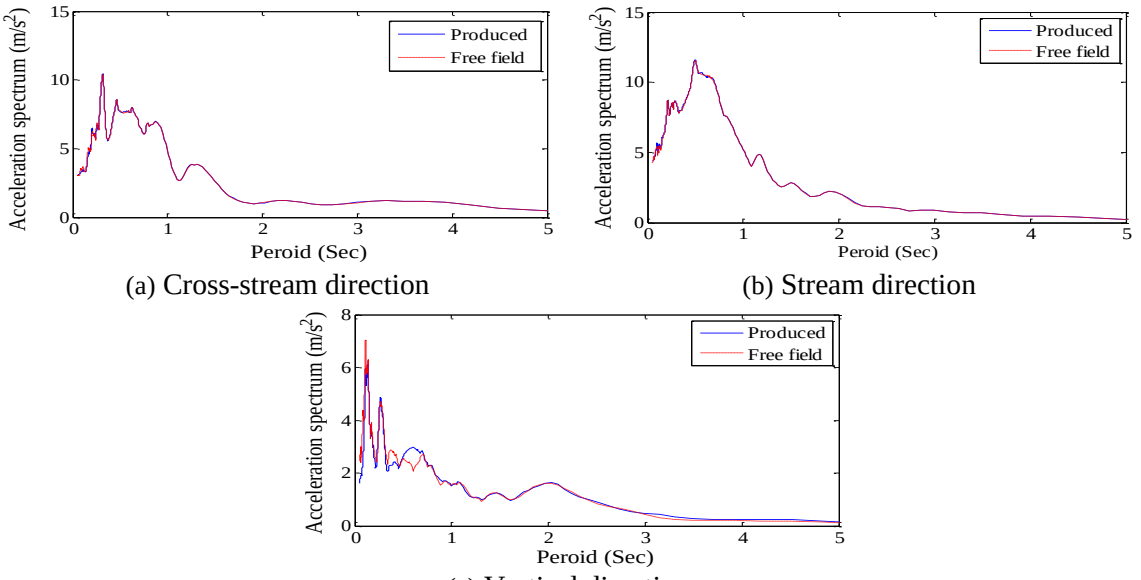

Fig. 14 Comparison between the response spectra of deconvolved earthquake ground acceleration on reference point and the corresponding target ones

5.1 Displacement results

Fig. 15 compares the crest displacements of the dam body in the cross-stream, stream, and

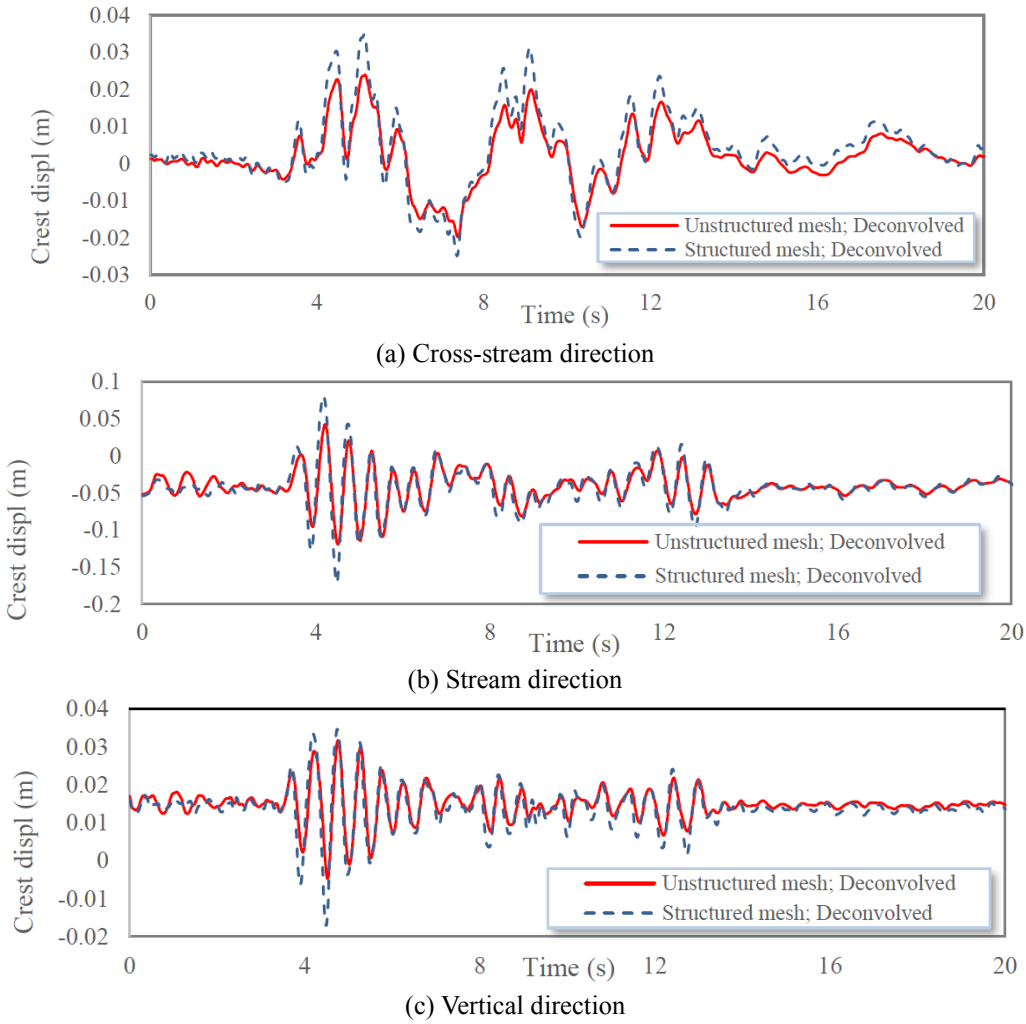

Fig. 15 Comparing crest displacements in three directions for different mesh types of the foundation; Deconvolved model

vertical directions, respectively. As can be seen, the frequency content of the crest response in both models is thoroughly the same. However, modelling foundation as an unstructured mesh decreases the maximum crest displacements in horizontal and vertical directions by 30% and 5% (=(A-B)/A×100, A: structured, B: unstructured) respectively. On the other hand, the crest displacements of the dam body in three directions for different mesh types of the foundation due to non-deconvolved earthquake input model are depicted in Fig. 16. It is worth noting that when the system is excited with the free-field acceleration time histories applied to the dam-foundation interface, the crest displacements in all three directions are not affected by mesh type of the foundation (as observed in Fig. 16). The reason for this is due to the fact that for the system under deconvolved input excitation, the earthquake waves propagate vertically from the bed rock toward the dam within the foundation medium. So it is expected that the mesh type of the foundation affects the displacement results. It is noteworthy that the CPU time for analysing models with structured

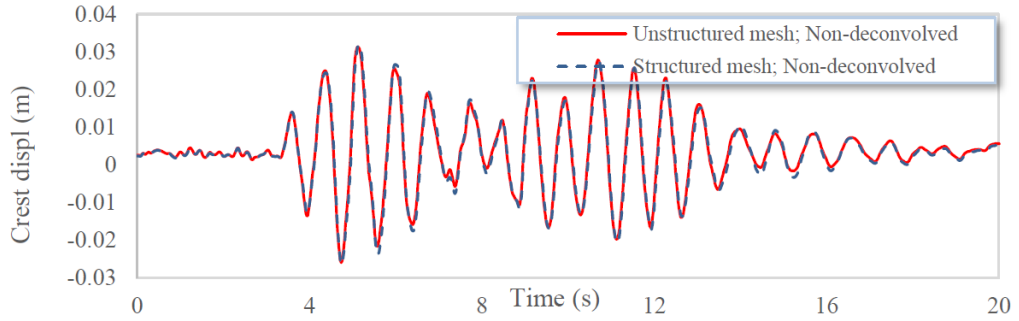

(a) Cross-stream direction

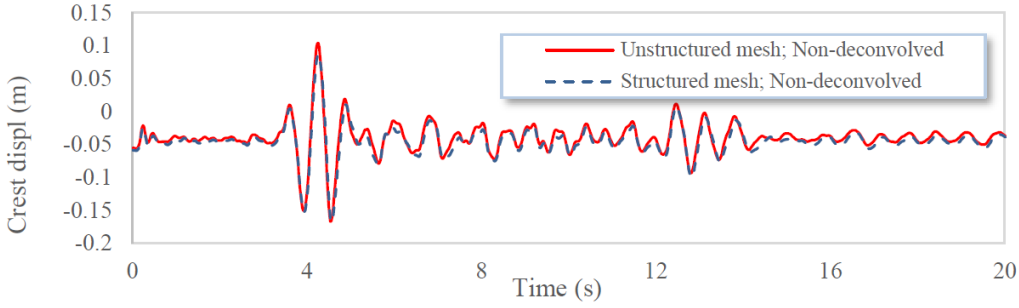

(b) Stream direction

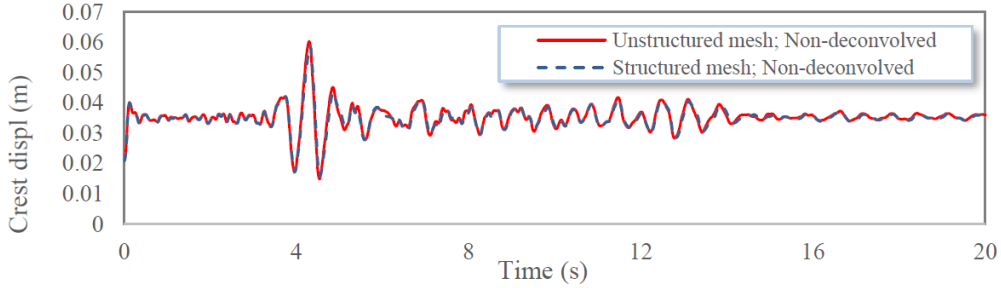

(c) Vertical direction

Fig. 16 Comparing crest displacements in three directions for different mesh types of the foundation; Non-deconvolved earthquake input model

foundation is twice as much as that of the unstructured models.

5.2 Stress results

Figs. 17 and 18 show the non-concurrent envelope of the first and third principal stresses, respectively on the upstream/downstream faces of the dam body. Generally, when the free-field ground motions are applied directly to the dam-foundation interface, the tensile overstressed areas appear on the upstream face of the dam body near the abutments in both structured and unstructured mesh foundation models. Instead, in the deconvolved earthquake input models, the tensile overstressed areas are extended along the dam-foundation interface. On the other hand, modelling foundation as unstructured mesh has no effect on both the intensity and extension of the tensile overstressed areas except for stress concentration at very small areas at the right lower abutment in

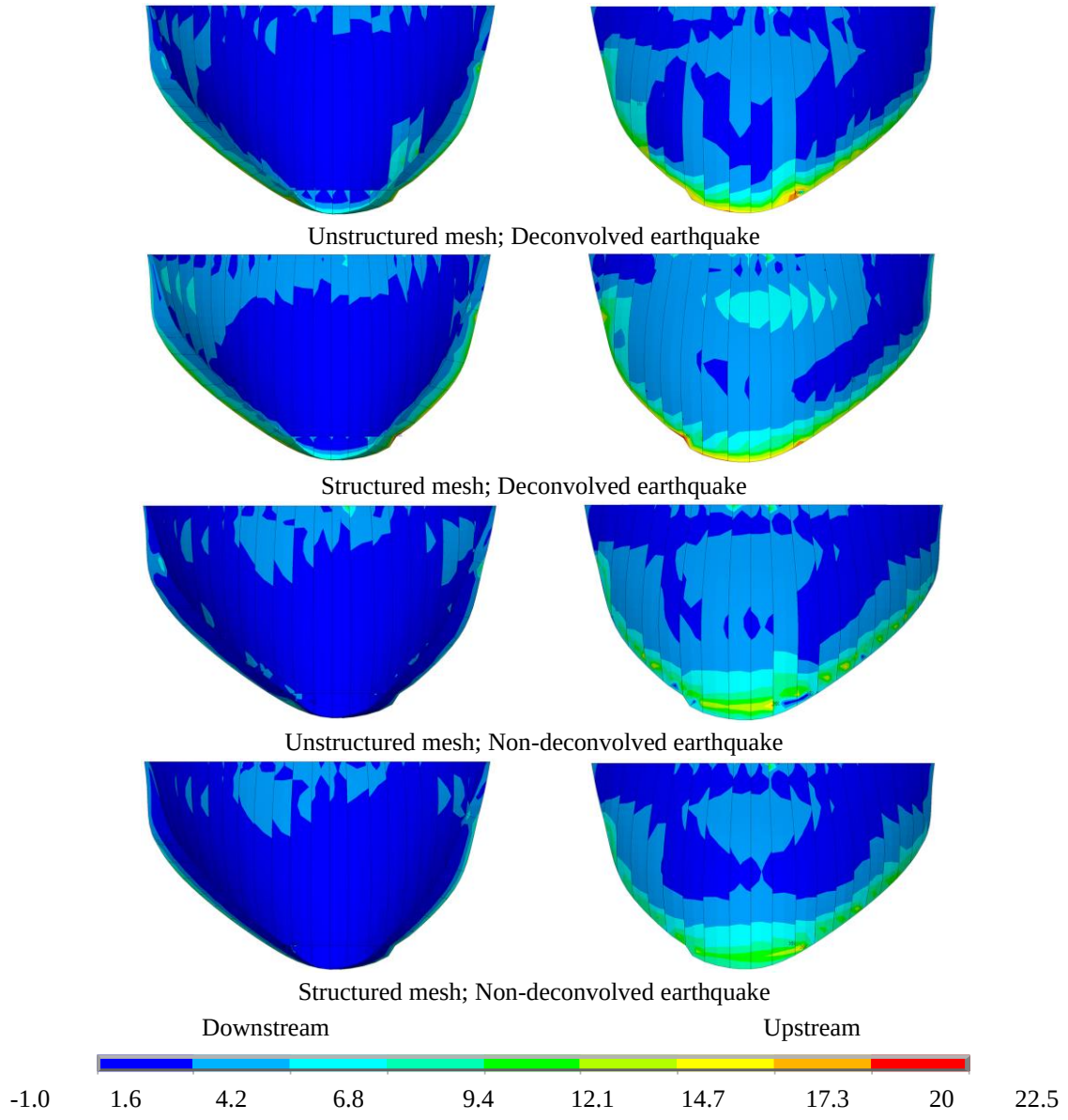

Fig. 17 Non-concurrent envelope of first (tensile) principal stresses on upstream and downstream faces of the dam body for different mesh types of the foundation under different earthquake input mechanisms (MPa)

comparison with the models using structured mesh foundation. It is worth noting that the highest compressive stresses resulted from the analyses are within the allowable limits (See Table 2). So, no crushing of the concrete would be expected for all cases. In addition, in the models with unstructured foundation the maximum compressive stresses decreased by 20% in comparison with those of the structured foundation models. Fig. 19 illustrates the tensile overstressed areas on the upstream and downstream faces of the dam body for different mesh types of the foundation and different earthquake input mechanisms. It can be observed from the Fig. 19 that in the structured

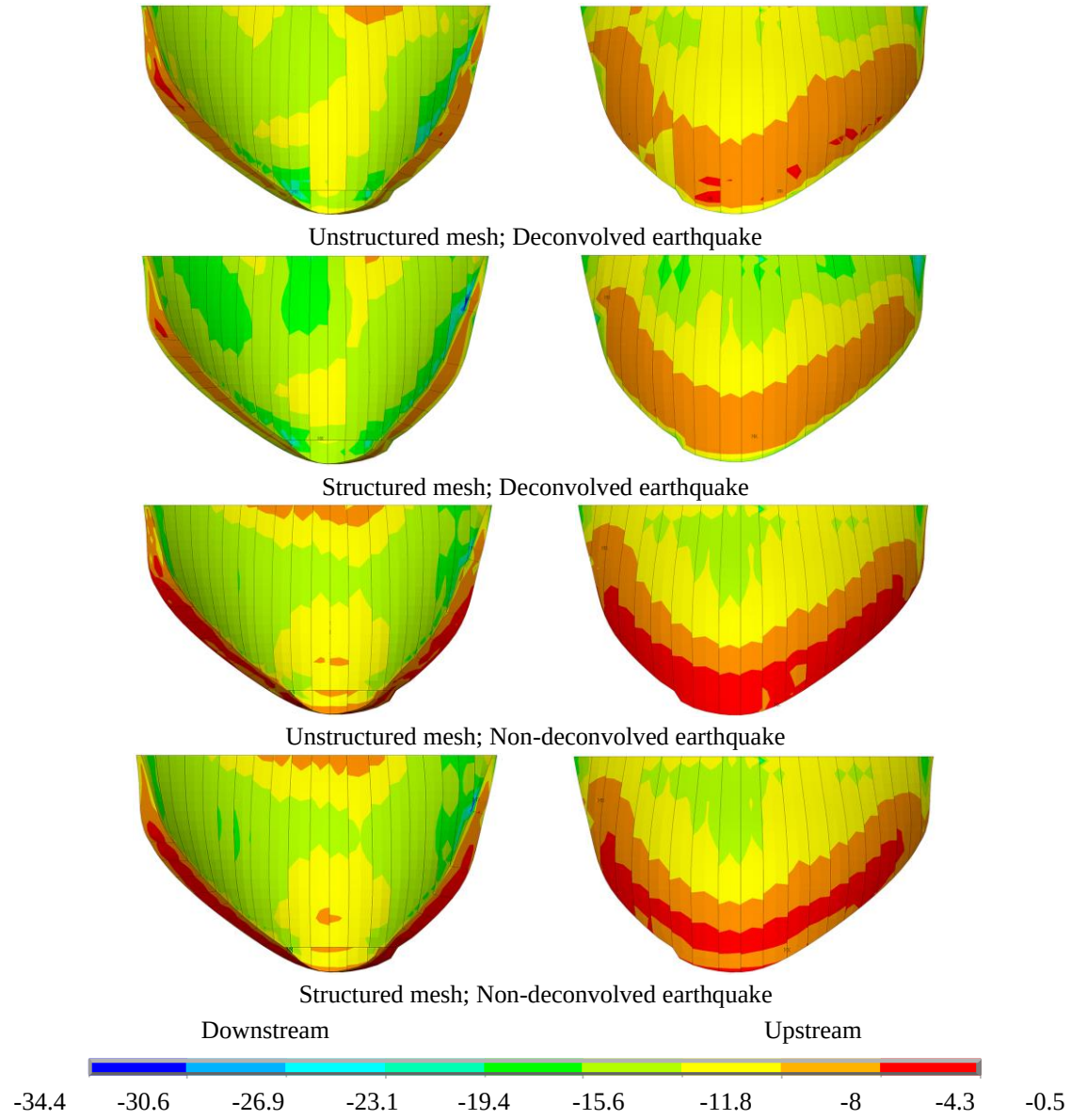

Fig. 18 Non-concurrent envelope of third (compressive) principal stresses in upstream and downstream faces of the dam body for different mesh types of the foundation under different earthquake input mechanisms (MPa)

mesh foundation model under deconvolved input excitation, the tensile overstressed areas extended slightly to the right abutment near the crest and very small areas in the middle part on downstream face of the dam body in comparison with the case analyzed modelling foundation as unstructured. Finally, in the deconvolved earthquake input models foundation the maximum tensile and compressive stresses increased by 19% and 12%, respectively in comparison with those of the free-field input models. This is due to the site effect caused by local topographical and geological

Table 2 Maximum values of tensile/compressive stresses and joint opening/sliding within the dam body and crest displacements for different mesh types of the foundation under different earthquake input mechanisms

	Status	Deconvolved		Non-deconvolved	
		Structured mesh	Unstructured mesh	Structured mesh	Unstructured mesh
Crest displacement (m)	Cross-stream direction	0.034	0.024	0.031	0.031
	Stream direction	-0.17	0.12	-0.17	-0.17
	Vertical direction	0.034	0.032	0.06	0.06
Principal (MPa)	Tensile	22.5	22.2	18.8	19
	Compressive	-34.4	-27.7	-30.6	-25
Joint opening/sliding (mm)	Opening	6.4	4.1	3.9	7.4
	Sliding	13.3	34.9	4	12

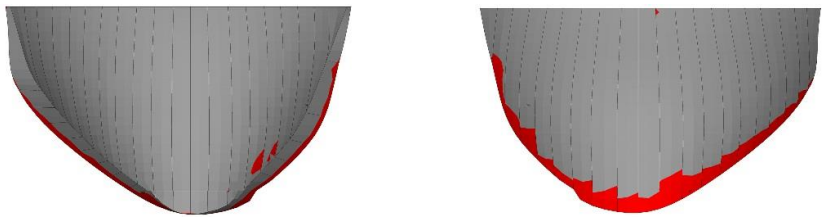

Unstructured mesh; Deconvolved earthquake

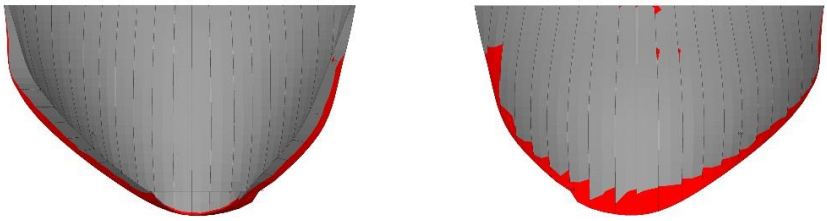

Structured mesh; Deconvolved earthquake

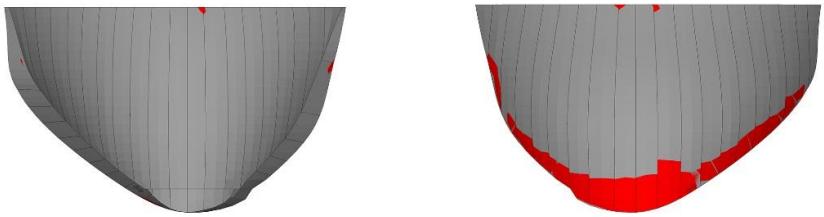

Unstructured mesh; Non-deconvolved earthquake

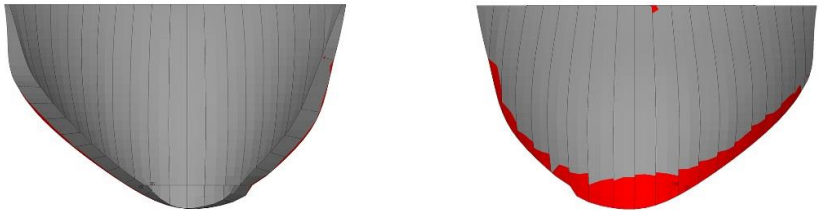

Structured mesh; Non-deconvolved earthquake

Downstream Upstream

Fig. 19 Overstressed areas of the first principal stresses in upstream and downstream faces of the dam body for different mesh types of the foundation under different earthquake input mechanisms

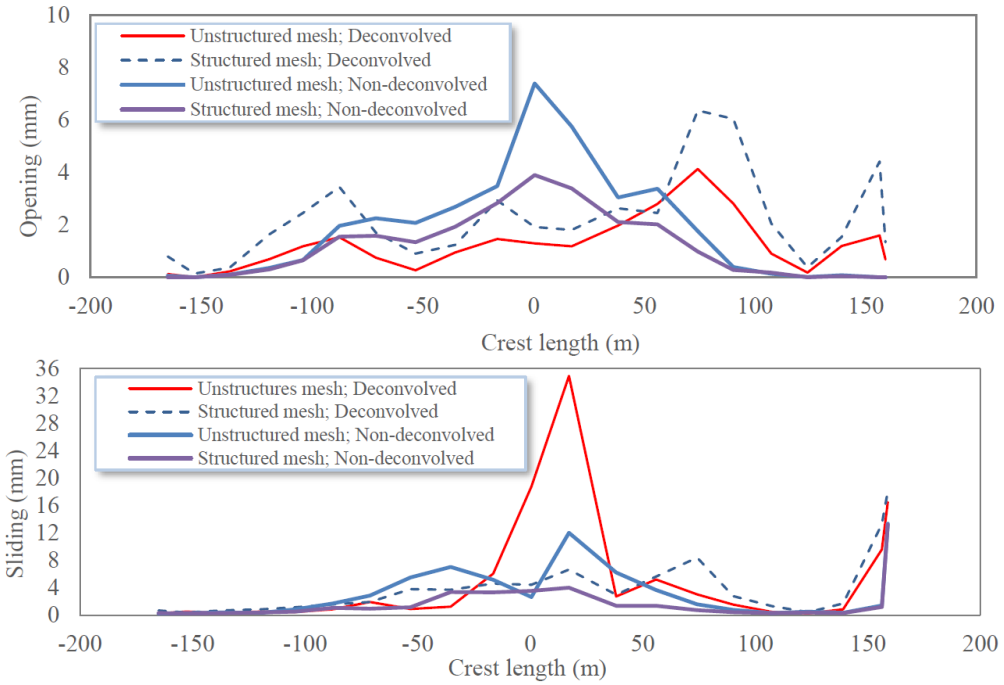

Fig. 20 Extreme values for joint opening/sliding; experienced by the upstream contact elements along the crest of the dam body for different mesh types of the foundation under different earthquake input mechanisms (mm)

behavior of foundation rock. Modelling foundation using structured mesh under inappropriate earthquake input mechanism leads to more conservative results in terms of stress levels and consequently in some cases may leads to an erroneous conclusion.

5.3 Performance evaluation

The seismic performance evaluation of concrete dams in the case of linear elastic analysis are based on indicators such as percentage of area overstressed, the cumulative inelastic duration and demand-capacity ratio (DCR). Based on the guideline, if the percentage of the overstressed (DCR=1) area on the dam face exceeds 20% of the total area, nonlinear analysis is recommended (USACE 2007). According to Fig. 19, in all cases, the percentage of the overstressed areas are located within the specified limit and so, the system does not need to be modeled considering material nonlinearity.

5.4 Joint opening and sliding

Fig. 20 shows the extreme values of joints opening/sliding experienced by contact elements located on the upstream face along the crest of the dam body. The maximum joint sliding occurs in the middle part of the crest as a leap in the unstructured models which is tripled in comparison with those of structured foundation models. Also, the maximum joint opening is pertinent to the unstructured model under non-deconvolved earthquake input as 7.4mm. The figures exhibit high differences in the middle part of the dam body while the figures for the joint sliding plateaued on the right hand of the dam body.

6. Conclusions

The present paper aims to study nonlinear seismic response of an existing arch dam subjected to different earthquake input mechanisms considering effects of different mesh types of the rock foundation. Nonlinearity originates from the opening/slipping of the vertical contraction joints within the dam body. The Karoun-I double curvature arch dam was selected as the case study. Two methods of the structured and unstructured mesh generations are used to model the foundation of the dam. The reservoir-structure interaction is taken into account via the finite element solution assuming compressible reservoir considering appropriate conditions around the boundaries. The viscous condition at the far-end boundary of the massed foundation is used to model the radiation effect. Three components of the 1994 Northridge earthquake are selected as the free-field ground motions. In the deconvolved earthquake input models, the analysis is carried out in two steps. First a deconvolution analysis is performed to adjust the amplitude and frequency contents of an earthquake ground motion applied to the base of the foundation model to achieve the desired ground acceleration at the dam-foundation interface at the different points. Then, the deconvolved acceleration history is applied to the foundation base of the dam-reservoir-foundation system to perform the seismic analysis. Based on the results, the spectra of the response at the dam-foundation interface at different points match very closely with the spectra of the horizontal free-field ground motions.

The main focus of the present paper is to study nonlinear seismic response of an existing arch dam subjected to different earthquake input mechanisms considering effects of different meshes for the surrounding foundation, in addition to both the joints nonlinearity and massed foundation phenomena, which is expected leading to more realistic results especially for geologically complex foundations. The main conclusions of the present work can be summarized as following:

1. In the deconvolved earthquake input models foundation the maximum tensile and compressive stresses increased by 19% and 12%, respectively in comparison with those of the free-field input models. This is due to site effect caused by local topographical and geological behavior of the foundation rock.
2. The frequency content of the crest response in all models is thoroughly the same. However, modelling foundation as unstructured mesh decreases the maximum crest displacements in the horizontal and vertical directions by 30% and 5% respectively, in comparison with those of the structured mesh model. On the other hand, when the system is excited with the free-field acceleration time history (applied to the dam-foundation interface), the crest displacements in all three directions are not affected by mesh type of the foundation.
3. For both structured and unstructured mesh foundation models, when the free-field ground motions are applied directly at the dam-foundation interface, the tensile overstressed areas appear on the upstream face of the dam body near the abutments. While, by applying of deconvolved earthquake input mechanism the tensile overstressed areas are extended along the dam-foundation interface.
4. Modelling foundation as unstructured mesh has no effect on both the intensity and extension of the tensile overstressed areas except for stress concentration at very small areas at the right lower abutment in comparison with the models with structured mesh foundation.
5. In the models with unstructured mesh foundation, the maximum compressive stresses decreases by 20% in comparison with those of the structured foundation models.
6. The present work demonstrates the possibility of using a structured mesh for the dam body and an unstructured meshing for the rock foundation under a suitable mechanism of the deconvolved earthquake input, and shows that the results are different and more reliable than the full use of a structured meshing for both dam and foundation subjected to the free-field motion

applied directly to the dam-foundation interface.

7. Modelling foundation using structured mesh under inappropriate earthquake input mechanism leads to more conservative results in terms of stress levels or displacements and consequently in some cases may leads to an erroneous decision and conservative design.

References

Andonov, A., Iliev, A. and Andreev, S. (2012), "Applicability of non-linear static procedures for seismic assessment of concrete dams", *Proceedings of the 15th World Conference on Earthquake Engineering*, Lisbon, Portugal, September.

ANSYS Version 11.0.1. (2007), Reference Manual, ANSYS Inc, Canonsburg, USA.

Benzley, S.E., Perry, E., Merkley, K., Clark, B. and Sjaardama, G. (1995), "A comparison of all hexagonal and all tetrahedral finite element meshes for elastic and elasto-plastic analysis", *Proceedings of the 4th International Meshing Roundtable*, Albuquerque, New Mexico, USA, October.

Buffi, G., Manciola, P., De Lorenzis, L., Cavalagli, N., Comodini, F., Gambi, A., ... & Tamagnini, C. (2017), "Calibration of finite element models of concrete arch-gravity dams using dynamical measures: The case of Ridracoli", *Procedia Eng.*, **199**, 110-115. https://doi.org/10.1016/j.proeng.2017.09.169.

Carl, J., Müller-Hoeppe, D. and Meadows, M. (2006), "Comparison of tetrahedral and brick elements for linear elastic analysis", University of Colorado Boulder, Boulder, USA.

Chandrupatla, T.R., Belegundu, A.D., Ramesh, T. and Ray, C. (2002), *Introduction to Finite Elements in Engineering*, 4th Edition, Prentice Hall, Upper Saddle River, NJ.

Chuhan, Z., Jianwen, P. and Jinting, W. (2009). "Influence of seismic input mechanisms and radiation damping on arch dam response", *Soil Dyn. Earthq. Eng.*, **29**(9), 1282-1293. https://doi.org/10.1016/j.soildyn.2009.03.003.

Cifuentes, A.O. and Kalbaug, A. (1992), "A performance study of tetrahedral and hexahedral elements in 3d finite element structural analysis", *Finite Elem. Anal. Des*., **12**(3-4), 313-318. https://doi.org/10.1016/0168-874X(92)90040-J.

Diwan, A.G. and Mahajan, Y.S. (2017), "Study of the effect of various parameters on the result of stress analysis obtained using tetrahedral and hexahedral mesh elements", *J. Chin. Inst. Eng.*, **40**(2), 101-109. https://doi.org/10.1080/02533839.2017.1287596.

FERC (1999), Engineering Guidelines for the Evaluation of Hydropower Projects: Chapter 11-Arch Dams, Federal Energy Regulatory Commission, Washington D.C. USA.

Gracia Llinares, L. (2016), "Development of a computational tool for structural verification of dams", Master's Thesis, Universitat Politècnica de Catalunya, Spain.

Hadzalic, E., Ibrahimbegovic, A. and Dolarevic, S. (2018), "Failure mechanisms in coupled soil-foundation systems", *Coupl. Syst. Mech.*, **7**(1), 27-42. https://doi.org/10.12989/csm.2018.7.1.027.

Hall, J.F. (2006), "Problems encountered from the use (or misuse) of Rayleigh damping", *Earthq. Eng. Struct. Dyn*., **35**(5), 525-545. https://doi.org/10.1002/eqe.541.

Hariri-Ardebili, M.A. and Mirzabozorg, H. (2012), "Seismic performance evaluation and analysis of major arch dams considering material and joint nonlinearity effects", *Int. Scholar. Res. Notice.*, **2012**, 1-10. http://doi.org/10.5402/2012/681350.

Hariri-Ardebili, M.A., Mirzabozorg, H. and Ghasemi, A. (2013), "Strain-based seismic failure evaluation of coupled dam-reservoir-foundation system", *Coupl. Syst. Mech.*, **2**(1), 85-110. http://dx.doi.org/10.12989/csm.2013.2.1.085.

Hariri Ardebili, M.A. and Saouma, V. (2013), "Impact of near-fault vs. far-field ground motions on the seismic response of an arch dam with respect to foundation type", *Dam Eng. J.*, **24**(1), 19-52.

Huang, J. and Zerva, A. (2014), "Earthquake performance assessment of concrete gravity dams subjected to spatially varying seismic ground motions", *Struct. Infrastr. Eng.*, **10**(8), 1011-1026. https://doi.org/10.1080/15732479.2013.782323.

Javidinejad, A. (2012), "FEA practical illustration of mesh-quality-results differences between structured mesh and unstructured mesh", *ISRN Mech. Eng.*, **2012**, 1-7. https://doi:10.5402/2012/168941.

Jin, A.Y., Pan, J.W., Wang, J.T. and Zhang, C. (2019), "Effect of foundation models on seismic response of arch dams", *Eng. Struct.*, **188**(1), 578-590. https://doi.org/10.1016/j.engstruct.2019.03.048.

Léger, P. and Boughoufalah, M. (1989), "Earthquake input mechanisms for time-domain analysis of dam-foundation systems", *Eng. Struct.*, **11**(1), 37-46. https://doi.org/10.1016/0141-0296(89)90031-X.

Lemos, J.V. (2012), *Modelling the Failure Modes of Dams' Rock Foundations*, Chapter 14, Italy.

Mirzabozorg H. (2014*), Final Report on Structural Study of Heightening Normal Level of Shahid Abbaspour Arch Dam*, 2nd Edition, Power Ministry, Tehran, Iran. (in Persian)

Mirzabozorg, H., Ghaemian, M., Noorzad, A. and Abbasi Zoghi, M. (2007), "Dam-reservoir-foundation interaction effects on nonlinear seismic behavior of concrete gravity dams using damage mechanics approach", *Int. J. Earthq. Eng. Eng. Seismol. (EEE)*, **3**, 52-60.

Owen, S.J. (1998), "A survey of unstructured mesh generation technology", *Proceedings of the 7th International Meshing Roundtable*, Dearborn, Michigan, USA, May.

Pacific Earthquake Engineering Research Centre (PEER) (2016), PEER Ground Motion Database, University of California, Berkeley, USA.

Pan, J., Zhang, C., Wang, J. and Xu, Y. (2009), "Seismic damage-cracking analysis of arch dams using different earthquake input mechanisms", *Sci. China Ser. E: Technol. Sci.*, **52**(2), 518-529. https://doi.org/10.1007/s11431-008-0303-6.

Ramezani, O., Mirzabozorg, H., Roohezamin, A.H. and Alimohammadi, M. (2017), "Critical time determination and solar radiation effect investigation of arch dams through mathematical and experimental thermal analysis", *Dam Eng. J.*, **XXVII**(4), 1-38.

Ramos, A. and Simões, J.A. (2006), "Tetrahedral versus hexahedral finite elements in numerical modeling of the proximal femur", *Med. Eng. Phys.*, **28**(9), 916-924. http://doi.org/10.1016/j.medengphy. 2005.12.006.

Saouma, V., Hansen, E. and Rajagopalan, B. (2001), "Statistical and 3D nonlinear finite element analysis of Schlegeis dam", *Proceedings of the Sixth ICOLD Benchmark Workshop on Rumerical Analysis of Dams*, Austria, October.

Schnabel, P.B., Lysmer, J. and Seed, H.B. (1972), SHAKE: A Computer Program for Earthquake Response Analysis of Horizontally Layered Sites, UCB/EERC-72/12, Earthquake Engineering Research Center, University of California, Berkeley.

Sevim, B., Altunışık, A.C. and Bayraktar, A. (2014), "Construction stages analyses using time dependent material properties of concrete arch dams", *Comput. Concrete*, **14**(5), 599-612. http://doi.org/10.12989/cac.2014.14.5.599.

Sooch, G.S. and Bagchi, A. (2012), "Effect of seismic wave scattering on the response of dam-reservoir-foundation systems", *Proceedings of the 15th World Conference on Earthquake Engineering*, Lisbon, Portugal, September.

USACE (2007), Earthquake Design and Evaluation of Concrete Hydraulic Structures, Report No: EM 1110-2-6053, United States Army Corps of Engineers, Washington, D.C.

USBR (2002), Static and Dynamic Linear Elastic Structural Analysis, (EACD3D96), Morrow Point Dam, United States Bureau of Reclamation, Denver, CO.

Vezi, M. (2014), "Dynamic modelling of arch dams in the ambient state", PhD Dissertation, University of Cape Town, Cape Town, South Africa.

Wang, E., Nelson, T. and Rauch, R. (2004), "Back to elements - tetrahedral vs. hexahedral", *Proceedings of the International ANSYS Conference*, ANSYS Pennsylvania.

Weingarten, V.I. (1994), "The controversy over hex or tet meshing", *Mach. Des.*, **66**(8), 74-77.

Ziaolhagh, S.H., Goudarzi, M. and Sani, A.A. (2016), "Free vibration analysis of gravity dam-reservoir system utilizing 21 node-33 Gauss point triangular elements", *Coupl. Syst. Mech.*, **5**(1), 59-86. http://doi.org/10.12989/csm.2016.5.1.059.